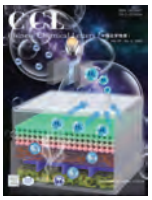
Chinese Chemical Letters 37 (2026) 111174

Contents lists available at ScienceDirect

Chinese Chemical Letters

journal homepage: www.elsevier.com/locate/cclet



Modulating the solvation sheath *via* bio-inspired electrolyte additives towards dendrite-free aqueous zinc ion batteries

Sida Zhang[a], Huaping Mei[b,c], Baoyu Li[d,*], Feilin Yu[b], Kaxin Wang[b], Ruduan Yuan[b], Ziga Luogu[b], Zhixian Zhang[f], Xiqian Hu[a], Jianxin Wang[a], Xuetao Duan[a], Pinyi Wang[a], Wanlong Wu[e], Qianzhi Gou[c,*], Meng Li[b,*], Weigen Chen[a,*]

[a] *State Key Laboratory of Power Transmission Equipment Technology, School of Electrical Engineering, National Innovation Center for Industry-Education Integration of Energy Storage, Chongqing University, Chongqing 400044, China*
[b] *National Innovation Center for Industry-Education Integration of Energy Storage, MOE Key Laboratory of Low-grade Energy Utilization Technologies and Systems, CQU-NUS Renewable Energy Materials & Devices Joint Laboratory, College of Energy & Power Engineering, Chongqing University, Chongqing 400044, China*
[c] *School of Building Services Science and Engineering, Xi'an University of Architecture and Technology, Xi'an 710055, China*
[d] *State Key Laboratory of Radiation Medicine and Protection, School for Radiological and Interdisciplinary Sciences (RAD-X) and Collaborative Innovation Center of Radiation Medicine of Jiangsu Higher Education Institutions, Soochow University, Suzhou 215123, China*
[e] *Shaanxi Key Laboratory of Chemical Reaction Engineering, School of Chemistry and Chemical Engineering, Yan'an University, Yan'an 716000, China*
[f] *School of Electrical and Electronic Engineering, Chongqing University of Technology, Chongqing 400054, China*

ARTICLE INFO

Article history:
Received 7 January 2025
Revised 22 March 2025
Accepted 2 April 2025
Available online 3 April 2025

Keywords:
Aqueous zinc-ion batteries
Electrolyte additive
Bio-inspired design concept
Zn metal anode
Solvation sheath

ABSTRACT

Aqueous zinc-ion batteries (AZIBs) have drawn numerous attention due to their low cost and environmental benefits. However, its commercialization process was hindered by issues, such as uncontrolled dendrite growth and parasitic side reactions. Inspired by the natural interaction between Zn^{2+} and amino acid chains in zinc finger proteins, we introduced L-proline (LP), a cost-effective additive, into the aqueous electrolyte to stabilize the Zn anode. In combination with experiments and theoretical calculation results, it is demonstrated that the LP additive tends to reshape the hydrated Zn^{2+} solvation sheath and weaken the free H_2O activity, thereby restricting the water-induced parasitic reactions and drastic dendrite growth. Therefore, the Zn symmetrical cells with LP-containing electrolytes delivered an excellent superior electrochemical performance, including a long-term calendar lifespan of 3400 h at 2 mA/cm^2 and nearly 450 h at 5 mA/cm^2. Meanwhile, the as-assembled Zn||MnO_2 full cells also showed desired cycling stability and rate performance with the assistance of LP additive, outperforming the $ZnSO_4$ system. This intriguing bio-inspired strategy provides a valuable insight for improving the longevity of AZIBs and advancing their development in energy storage.

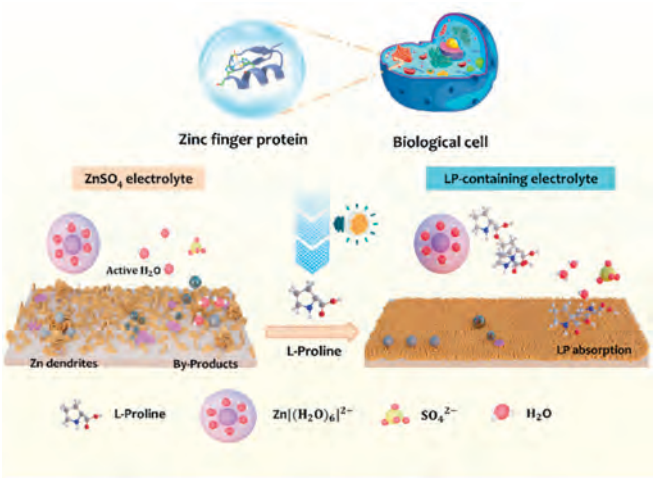
© 2026 Published by Elsevier B.V. on behalf of Chinese Chemical Society and Institute of Materia Medica, Chinese Academy of Medical Sciences.

In recent years, aqueous zinc-ion batteries (AZIBs) have attracted considerable attention as a promising alternative for energy storage systems [1–4]. Compared to lithium-ion batteries, AZIBs possess various merits, including abundant resources, low cost environmental friendliness, and relatively high theoretical capacities (820 mAh/g and 5855 mAh/cm^3) [5–7]. However, the Zn metal anode in aqueous systems still faces significant challenges due to its complex interfacial reactions. Generally, major issues include persistent hydrogen evolution reactions (HER), zinc corrosion, and the "tip effect" linked to dendritic growth, all of which undermine the long-term stability and cycling performance of the batteries [8,9].

To tackle these challenges, tremendous efforts have been proposed to stabilize the Zn anodes, focusing on strategies such as surface engineering [10,11], regulating zinc electrodeposition [12], developing advanced separators [5,13,14], and incorporating electrolyte additives [15–17]. Among these methods, electrolyte additives have gained prominence due to its simplicity and effectiveness in stabilizing Zn anodes by reconstructing the Zn^{2+} solvation sheath [18–20]. Generally, the coordination of water molecules with solvated Zn^{2+} ions is a critical factor driving parasitic side reactions during the electrodeposition process. Additionally, an uneven Zn^{2+} flux at the anode-electrolyte interface (AEI) can lead to dendrite formation, further deteriorating battery performance

* Corresponding authors.
E-mail addresses: byli@suda.edu.cn (B. Li), gqz813@xauat.edu.cn (Q. Gou), limeng@cqu.edu.cn (M. Li), weigench@cqu.edu.cn (W. Chen).

https://doi.org/10.1016/j.cclet.2025.111174
1001-8417/© 2026 Published by Elsevier B.V. on behalf of Chinese Chemical Society and Institute of Materia Medica, Chinese Academy of Medical Sciences.



Scheme 1. The schematic illustration of LP additive and related working mechanisms on Zn anode.

[21,22]. To mitigate these issues, various additives have been introduced into aqueous medium to stabilize the Zn anode. For example, *N*,*N*-dimethyl acetamide, with its high hydrogen bond donor number, exhibits a strong affinity for coordinating with Zn^{2+}, thereby reducing the reactivity of the hydrogen evolution reaction [18]. Similarly, the addition of 10 mmol/L glucose has demonstrated the ability to improve the reversibility of Zn plating/stripping by effectively minimizing the disruptive influence of water molecules on Zn^{2+} solvation shell [23]. Furthermore, amphoteric poly(acrylic acid), an organic solvent additive, exhibits a high binding affinity for Zn^{2+}, effectively reshaping its solvation sheath and suppressing undesired side reactions [24–26]. However, most additives show limited efficacy at high current densities, a critical condition for practical applications [27]. Additionally, the incorporation of combustible or environmentally hazardous organic additives could compromise the intrinsic safety and eco-friendliness of AZIBs [28–30]. Despite these advancements mark significant progress, further research is essential to develop scalable, safe, and sustainable solutions for stabilizing Zn anodes under demanding operational conditions [31–33].

Nature offers valuable insights into optimizing ionic transport [33–35]. In eukaryotic cells, Zn^{2+} exhibits a strong affinity for amino acids, forming zinc finger proteins (ZFP) through tetrahedral coordination with specific residues, a property that underscores its ability to create stable complexes [16,36]. In the aqueous electrolytes, Zn^{2+} is coordinated within a solvation sheath of six water molecules, which can hinder its diffusion, de-solvation, and deposition processes. To address this issue, modulating the water molecules in the solvated sheath has emerged as a promising strategy. Inspired by the unique zincophilic mechanisms of ZFP, incorporating amino acids as electrolyte additives could replace solvated water molecules, intelligently regulating Zn^{2+} transport, modulating its deposition and stabilizing the interfacial chemistry [29,34,37]. This approach not only mitigates issues such as HER and dendrite formation but also enhances the stability and performance of the Zn anode, offering a creative bio-inspired design concept to enhance the efficiency and durability of AZIBs.

Herein, we proposed a facile strategy to stabilize the Zn metal anode *via* tailoring electrolyte solvation sheath with a kind of amino acid electrolyte additive (Scheme 1). More specifically, as a zincophilic compound, L-proline (LP) has been selected and adopted, enabling an unexpectedly stable Zn plating/stripping with an extended operation life of 3400 h at 2 mA/cm^2 and 450 h at 5 mA/cm^2, respectively. In combination with theoretical calculations and experimental test results, it is confirmed that the LP additive with zincophilic groups tends to confine proportion of free water and be absorbed on the anode in the aqueous environment, which is highly conducive to reducing the reaction activity. Meanwhile, the LP additive is also proven to be capable of replacing coordinated water molecules and participating in the solvated Zn^{2+} sheath, contributing to the restraint of dendrite growth and side reactions involved in interfacial reaction at the AEI during cycling. Besides, the feasibility of implementing electrolytes incorporating LP additives in AZIBs with MnO_2 cathodes was assessed, resulting in an outstanding initial discharging capacity of 119 mAh/g and exceptional capacity retention of 91.1 % after 500 cycles at 2.0 A/g. This strategy provides new insights into addressing the challenge of active water molecules in electrolytes and promotes the practical application of AZIBs.

In Fig. 1a, an LP molecule contains an amino and a carboxyl groups, which is expected to coordinate with Zn^{2+} by virtue of its natural zincophilicity. Firstly, the evolution of the electrolyte solvation structure is analyzed by spectroscopy and theoretical calculations, with 2 mol/L $ZnSO_4$ (ZSO) as the benchmark electrolyte and LP serving as the electrolyte additive (Fig. S1 in Supporting information), denoted LP30, LP50, LP100 and LP200, respectively. To investigate the solvation interactions, the nuclear magnetic resonance (NMR) spectrum was analyzed, as shown in Fig. 1b, well-defined signal at 4.74 ppm was observed for the ZSO electrolyte. Upon introducing the LP additive, the peak position shifted to 4.72 ppm, indicating an increase in electronic density [38,39]. This shift suggests the release of coordinated H_2O molecules and the formation of new hydrogen bonds networks between LP molecules and H_2O molecules [40]. To further clarify the solvation structures of different electrolytes, Raman spectra of $\nu(SO_4^{2-})$ for various electrolytes were examined (Fig. 1c). In accordance with the renowned Eigen-Tamm mechanism, the interactions between cations and anions in the electrolyte are classified into two distinct categories: solvent-separated ion pairs (SSIP) and contact ion pairs (CIP), respectively. As the additive concentration increases, the contribution of CIP gradually decreases, while the SSIP state becomes predominant [41,42]. This result indicates that SO_4^{2-} anions will rarely participate in the solvation structure upon the incorporation of LP molecules. Thus, the interaction between Zn^{2+} and SO_4^{2-} is significantly weakened due to the strong affinity between the LP additive and Zn^{2+}. According to Fourier transform infrared spectroscopy (FT-IR), with the addition of LP molecules, the stretching vibration of the O–H bond in water molecules shifts significantly to the lower wavenumber, while the bending vibration, ν(O–H), shifts markedly to the higher wavenumber (Figs. 1d and e). This observation indicates that LP molecules, which contain zincophilic groups, can reconstruct hydrogen bonds networks and interact with H_2O molecules, thereby reducing the free-water activity in the electrolyte [43]. To further confirm this mechanism, the electrochemical stability window of the LP-containing electrolyte is significantly enhanced compared to the ZSO electrolyte, particularly when the additive concentration reaches 100 mmol/L (Fig. 1f). Furthermore, electrochemical impedance spectra (EIS) of Ti symmetrical cells with various electrolytes reveals that the ionic conductivities of LP-modified electrolytes are slightly improved. This improvement may be attributed to the amphoteric nature of LP additives, which exhibit strong affinities in aqueous electrolytes. Based on these results, an optimal LP additive concentration of 100 mmol/L is selected to investigate its role in stabilizing the Zn anode. Density functional theory (DFT) calculations were further conducted to analyze the interaction behavior and binding energy between Zn^{2+}, water, and LP molecules. As depicted in Fig. 1g, the binding energy of the Zn^{2+}-LP complex is significantly larger than that of the Zn^{2+}-H_2O and H_2O-LP complexes, proving the preference for the participation of LP in the solvation sheath [44,45]. Moreover,

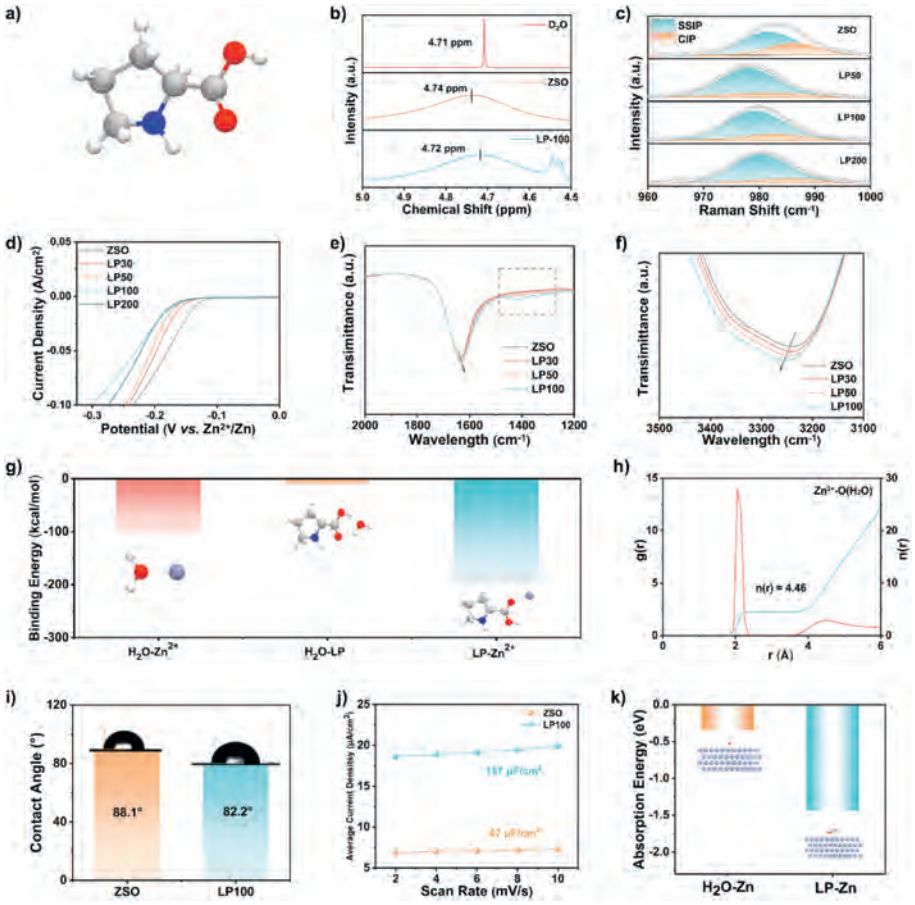


Fig. 1. (a) Molecular structural model of a LP (N atom: blue, C atom: gray, O atom: red, H atom: white). (b) ^{1}H NMR spectra of the ZSO and LP-containing electrolytes. (c) Raman spectra of the ZSO and LP-containing electrolytes. (d) LSV curve of the ZSO and LP-containing electrolytes. (e, f) FT-IR spectra of the ZSO and LP-containing electrolytes. (g) Binding energy between different species (Zn^{2+}, LP and H_2O). (h) Radial distribution functions (RDFs) (g(r)) and coordination number (n(r)) of Zn^{2+}-O (H_2O) in the LP100 electrolyte. (i) The WCAs between the ZSO and LP100 electrolytes on the Zn anode. (j) Average differential capacitance for Zn anode in the different electrolytes. (k) Absorption energy comparison of H_2O and LP molecules on Zn (002) crystal plane, insets show the corresponding absorbed models.

Fig. 1h illustrates the calculated n(r) values were 4.46 for Zn^{2+}-O (H_2O) and 0.01 for Zn^{2+}-O (LP), confirming the modulation of the solvation sheath for $[Zn(H_2O)_6]^{2+}$ with LP additive compared to the ZSO electrolyte (Figs. S2-S4 in Supporting information) [21,46]. In this scenario, the LP additive might perturb the original hydrogen bond network, leading to a reduction in H_2O–H_2O interactions [47]. To evaluate the wettability of the electrolytes on the Zn anode, water contact angles (WCAs) tests were performed. As illustrated in Fig. 1i, the WCAs value of ZSO (88.1°) was notably larger than that of LP100 (82.2°), suggesting a stronger interaction between the LP100 electrolyte and the Zn anode. Moreover, as depicted in Fig. 1j and Fig. S5 (Supporting information), an electric double-layer capacitance (EDLC) analysis was carried out. The LP100 electrolyte demonstrated a capacitance of 157 μF/cm^2, which was significantly larger than the ZSO electrolyte (47 μF/cm^2). This substantial improvement highlights the efficient adsorption of LP molecules onto the Zn anode as a dynamic layer, effectively modulating the Zn^{2+} electrodeposition process [29]. As shown in Fig. 1k, the calculated adsorption energy (E_{ads}) values for Zn-LP and Zn-H_2O interactions as −1.44 and −0.34 eV, respectively. These results indicate a stronger affinity of LP for the Zn anode, effectively blocking reactive sites for side reactions, promoting uniform Zn deposition, and suppressing dendrite growth.

A comprehensive evaluation of the extended cycling stability of Zn symmetrical cells was carried out using different electrolytes. Compared with the ZSO electrolyte, the symmetrical cells with the LP100 electrolyte demonstrated significantly enhanced cycle stability. The voltage profiles for Zn plating and stripping at a current density of 2 mA/cm^2 and a capacity of 1 mAh/cm^2 are illustrated in Fig. 2a. The ZSO electrolyte-based cell exhibits poor cycling stability, as evidenced by an abrupt voltage fluctuation around 150 h, likely caused by Zn dendrite penetration. In sharp contrast, the Zn symmetrical cell with the LP electrolyte exhibits outstanding performance, with stable voltage levels maintained for over 3400 h, demonstrating that LP additives effectively improve the cycle stability of Zn anode. Additionally, durability testing was performed at a current density of 5 mA/cm^2 and a capacity of 5 mAh/cm^2. Notably, the symmetrical cell assembled with the LP100 electrolyte showed a long-term cycle life of approximately 450 h, representing a significant improvement over the ZSO electrolyte (90 h) (Fig. 2b). As shown in Fig. S6 (Supporting information), Zn symmetrical cells with the LP100 electrolyte demonstrate remarkable cycling stability, enduring nearly 220 h of continuous operation at a high current density of 20 mA/cm^2 and a capacity of 8 mAh/cm^2, significantly outperforming the ZSO electrolyte, which lasts less than 70 h. Additionally, the rate performance of Zn symmetrical cells with different electrolytes is presented in Fig. 2c. As the current density increases from 1 mA/cm^2 to 8 mA/cm^2, the hysteresis voltage of the LP100 electrolyte cell is slightly higher than that of the ZSO electrolyte, mainly due to the strong interaction between Zn^{2+} and solvation sheath. This demonstrates the excellent reversibility of Zn plating/stripping process with LP incorporation, as confirmed by the consistent voltage profile. The increased polarization voltage and nucleation overpotential in the LP100 electrolyte promote

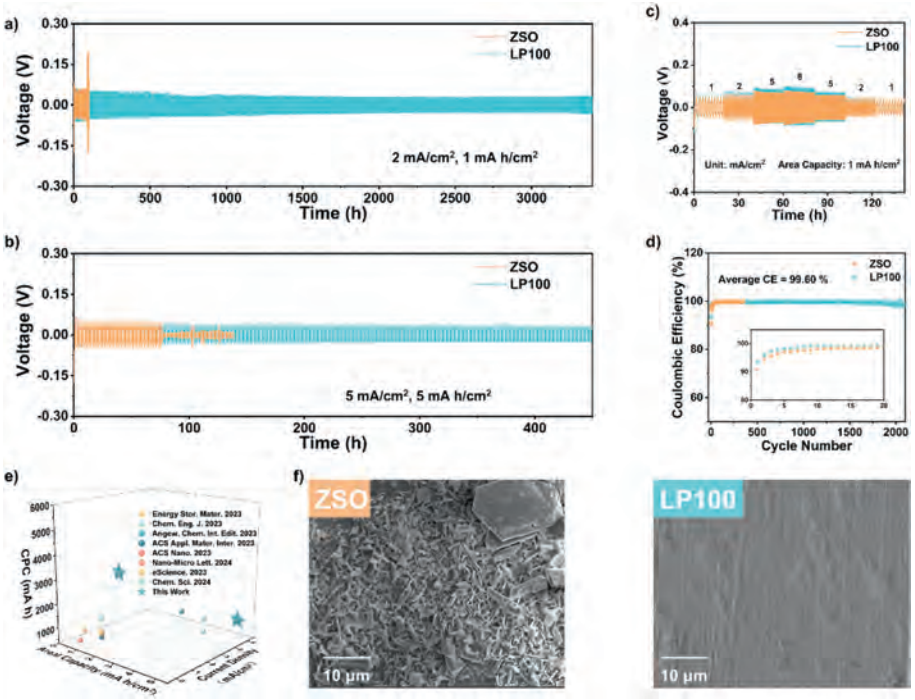


Fig. 2. (a) Galvanostatic charge/discharge (GCD) cycling of Zn symmetrical cells at 2.0 mA/cm^2, 1.0 mAh/cm^2 and (b) 5.0 mA/cm^2, 5.0 mAh/cm^2. (c) Rate performance and (d) the corresponding voltage hysteresis at various densities of Zn symmetrical cells. (e) CE test of Zn||Cu asymmetrical cells. CE test of Zn||Cu asymmetrical cells. SEM images of Zn anodes in the (f) ZSO and (g) LP100 electrolytes after 50 cycles at 2.0 mA/cm^2, 1.0 mAh/cm^2.

the formation of smaller Zn nuclei, leading to more uniform deposition (Figs. S7 and S8 in Supporting information). The reversibility of the Zn anode under different electrolyte conditions was evaluated through Zn plating and stripping tests in Zn||Cu asymmetrical cells at 2 mA/cm^2, 1 mAh/cm^2. As shown in Fig. 2d, the Zn||Cu cell with the LP100 electrolyte achieved an impressive average coulombic efficiency (CE) of 99.60% over 2000 cycles, significantly outperforming the ZSO electrolyte cell (Fig. S9 in Supporting information). Additionally, the initial CE of the Zn||Cu cell with LP100 electrolyte is 96.39%, notably higher than that of the ZSO electrolyte. The superior electrochemical performance of Zn||Zn symmetric cells using the LP100 electrolyte, excelling in comparison to several recent studies, suggests its potential application in AZIBs [18,47–53]. Furthermore, the corresponding scanning electron microscopy (SEM) images of Zn anode in the ZSO electrolyte reveal a dendritic morphology and some hexagonal byproducts on the Zn anode. In contrast, the Zn anode cycled in the LP100 electrolyte exhibits a smooth and dense morphology due to suppressing the generation of Zn dendrites and byproducts (Fig. 2f).

The corrosion protection performance of the LP additive on the Zn electrode was evaluated using Tafel plots. The Zn anode in the LP electrolyte showed a lower corrosion current density compared to the ZSO electrolyte, highlighting the ability of LP molecules to delay the onset of Zn anode corrosion (Fig. 3a). Furthermore, X-ray diffraction (XRD) analysis in Fig. 3b demonstrates that LP molecules effectively inhibit the formation of byproducts like $Zn_4SO_4(OH)_6{\cdot}xH_2O$ on the Zn anode. In addition to suppressing side reactions, the influence of LP molecules on Zn^{2+} deposition behavior at the AEI was further examined. Chronoamperometry (CA) was used to monitor the evolution of Zn nucleation and growth under an overpotential of −150 mV in Zn symmetrical cells (Fig. 3c). In the ZSO electrolyte, the rapid decrease in current density with time suggests that the Zn anode surface is controlled by 2D diffusion, where Zn^{2+} migrates along the anode, and the resulting "tip effect" promotes continuous Zn accumulation, leading to dendrite formation [54]. In contrast, the addition of LP molecules slow the current growth rate by limiting the 2D diffusion of Zn^{2+}. In the LP100 electrolyte, the Zn^{2+} flux at the electrode/electrolyte interface is effectively controlled, resulting in a stable 3D diffusion mode with the lowest current density response [7,55,56]. This observation confirms that LP molecules efficiently suppress byproduct formation, enabling prolonged dendrite-free cycling. To investigate the effect of LP molecules on stabilization, *in-situ* optical microscopy was employed to monitor changes at the electrode/electrolyte interface during Zn deposition. Finite element analysis using COMSOL software reveals that during the plating process, irregular micro-bumps form on the Zn electrode due to its uneven roughness (Fig. 3d). In the ZSO electrolyte, a clear intensity gradient in the electric field distribution on the Zn anode was observed, ranging from isolated nuclei to covering the entire surface, which increases over time (Fig. 3e). The localized electric field accelerates dendrite growth by concentrating charges at the tips of the bumps. However, zincophilic LP additives effectively inhibit dendrite formation by adsorbing onto the AEI, regulating electric field intensities, and promoting efficient deposition on concave surfaces. Additionally, these additives help control Zn^{2+} flux distributions, leading to varied deposition rates based on location (Fig. 3f). This results in uniform and compact Zn deposition, gradually filling the concave surfaces.

Subsequently, the Zn plating/stripping kinetics were investigated to further reveal the mechanism of Zn electrodeposition behavior with the effect of LP additive. First, we explored the effect of the increase of overpotential caused by the addition of LP molecules on the diffusion for Zn^{2+} at the AEI. As shown in Figs. S10-S12 (Supporting information), the activation energy (E_a) for interfacial Zn^{2+} transference was measured based on the resistance response over a temperature range from 303 K to 343 K. Generally, the E_a can be extracted from the fitting of the as-following Arrhenius equation:

$$\frac{1}{R_{ct}} = Ae^{\frac{-E_a}{RT}} \quad (1)$$

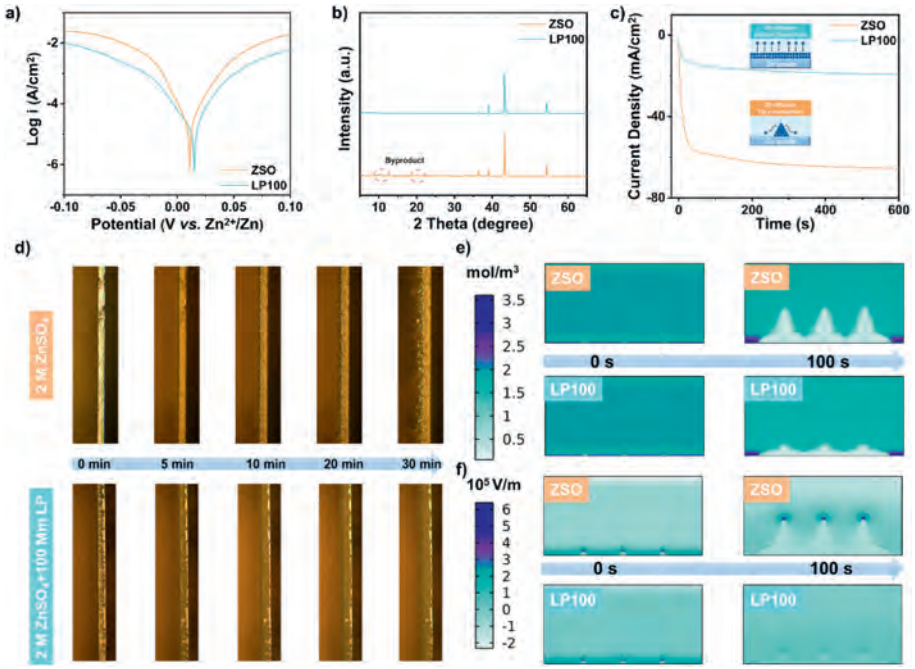


Fig. 3. (a) Tafel plots of the Zn anodes in the ZSO and LP100 electrolytes at 2 mV/s based on Zn symmetrical cells. (b) XRD patterns after immersing in the ZSO and LP100 electrolytes. (c) CA curves of Zn anode at −150 mV in the ZSO and LP100 electrolytes. (d) *In situ* optical observations of Zn deposition morphologies. COMSOL multiphysics simulation of Zn anode during plating for (e) Zn^{2+} flux and (f) electric field.

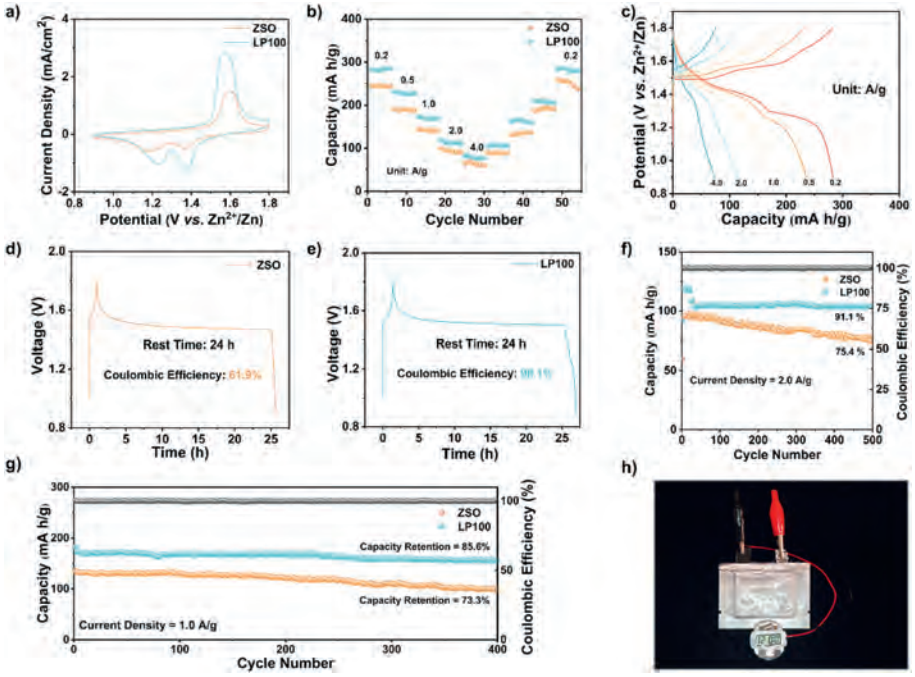


Fig. 4. (a) CV curves. (b) Rate performance. (c) GCD curves for Zn||MnO_2 full cell at different current densities in the LP100 electrolyte. (d) ZSO and (e) LP100 electrolytes when charged to 1.8 V, left idle for 24 h, and discharged to 0.9 V. (f) Cycling performance of Zn||MnO_2 full coin cells tested at the current density of 2.0 A/g. (g) Cycling performance of Zn||MnO_2 full pouch cells tested at the current density of 1.0 A/g. (h) Photograph of Zn||MnO_2 pouch cell.

where R_{ct} is the charge transfer resistance, A is the frequency factor, R is the gas constant, and T is the absolute temperature. After fitting, the cell using the ZSO electrolyte exhibits an E_a value of 37.74 kJ/mol. In addition, the E_a value of the cell with the LP-100 electrolyte decreased to 32.58 kJ/mol, signifying a substantial decrease in the barrier for hydrated Zn^{2+} de-solvation and an enhancement in Zn^{2+} deposition kinetics [57–59]. As depicted in Figs. S13-S16 (Supporting information), the Zn^{2+} transference number is calculated to be 0.69 in the ZSO electrolyte, higher than that for the ZSO electrolyte (0.48). This phenomenon is mainly ascribed to weakened Zn^{2+} solvation effect which improves the ion transference number in the LP100 electrolyte [30,60].

We evaluated the electrochemical performance of Zn||MnO_2 full cells with different electrolytes. The cyclic voltammetry (CV) curves of the Zn||MnO_2 cell at a scan rate of 0.2 mV/s with various electrolytes are shown in Fig. 4a. The Zn||MnO_2 full cell with the LP100

electrolyte exhibits less voltage polarization compared to the ZSO electrolyte, indicating improved reversibility after electrolyte modification [37]. The rate performance of the Zn||MnO_2 full cell was assessed at different current densities. As displayed in Fig. 4b, the LP100 electrolyte significantly enhances the rate capacity, delivering a high discharge capacity of 281.6 mAh/g at 0.2 A/g. It maintains specific capacities of 226.4, 169.4, 112.2, and 81.0 mAh/g at 0.5, 1.0, 2.0, and 4.0 A/g, respectively. The corresponding charge-discharge curves in Fig. 4c and Fig. S17 (Supporting information) further demonstrate the improved capacity of the full cell with the LP100 electrolyte. The incorporation of LP molecules effectively suppressed parasitic reactions, reducing self-discharge. As shown in Figs. 4d and e, the LP100 electrolyte-based full cell retained 98.1 % of its initial capacity after 24 h rest, exhibiting a significant improvement compared to the ZSO electrolyte cells, which retained only 61.9 %. Additionally, as shown in Fig. 4f, the long-term cycling performance of the full cells with different electrolytes was evaluated at a current density of 2.0 A/g. The Zn||MnO_2 full cell with LP100 electrolyte demonstrates superior cycle life and stability compared to the ZSO electrolyte. As shown in Fig. 4g, even with an ultrathin Zn anode (20 μm) and low N/P ration (4.8), the pouch cell (3 cm × 4 cm) exhibits excellent long-term cycling performance, maintaining a capacity of 156.7 mAh/g after 400 cycles at 1.0 A/g. As show in Fig. 4h, the pouch cell efficient power supply when used to drive a digital timer, illustrating the ability of LP molecules to reduce parasitic reactions and minimize energy loss.

In summary, inspired by the natural affinity between Zn^{2+} and amino acid chains in ZFPs, a cost-effective and environmentally friendly LP additive was introduced into the aqueous electrolyte to stabilize the Zn anode. Through a combination of theoretical calculations and electrochemical tests, LP plays a key role in modulating the interactions between Zn^{2+}, H_2O molecules, and SO_4^{2-}. Concretely, the LP molecules not only modify the solvation sheath by replacing coordinated H_2O molecules, but preferentially adsorb onto the Zn metal anode, preventing the “tip effect”. This promotes uniform Zn nucleation and dendrite-free deposition on the cycled Zn anode. Zn anodes can be cycled for 3400 h at 2.0 mA/cm^2 in the Zn symmetrical cell. By adopting the LP additive, the Zn||Cu asymmetrical cell achieves a high average CE of 99.60 % for over 2100 cycles at 2.0 mA/cm^2. Notably, the Zn||MnO_2 full cell exhibited excellent cycling stability and capacity retention after 400 cycles in a pouch cell, demonstrating the LP molecules show great potential in improving the applicability of AZIBs. Our findings present a simple and effective electrolyte design strategy, which can significantly contribute to the development of low-cost AZIBs commercialization.

Declaration of competing interest

The authors declare that they have no known competing financial interests or personal relationships that could have appeared to influence the work reported in this paper.

CRediT authorship contribution statement

Sida Zhang: Writing – review & editing, Writing – original draft, Software, Methodology, Investigation, Data curation, Conceptualization. **Huaping Mei:** Validation, Methodology. **Baoyu Li:** Writing – original draft, Software, Resources, Methodology. **Feilin Yu:** Investigation. **Kaxin Wang:** Formal analysis. **Ruduan Yuan:** Software, Resources. **Ziga Luogu:** Methodology, Data curation. **Zhixian Zhang:** Investigation. **Xiqian Hu:** Visualization, Formal analysis. **Jianxin Wang:** Formal analysis. **Xuetao Duan:** Methodology. **Pinyi Wang:** Investigation. **Wanlong Wu:** Validation, Methodology, Formal analysis. **Qianzhi Gou:** Writing – review & editing, Writing – original draft, Supervision. **Meng Li:** Writing – review & editing, Validation, Resources, Funding acquisition. **Weigen Chen:** Writing – review & editing, Writing – original draft, Visualization, Validation, Supervision, Software, Resources, Project administration, Methodology, Conceptualization.

Acknowledgments

This work was financially supported by research grants from the National Natural Science Foundation of China (Nos. 52307159 and 52173235), Innovative Research Group Project of National Natural Science Foundation of China (No. 52021004), the Hainan Province Science and Technology Special Fund (No. ZDYF2024SHFZ038), Venture & Innovation Support Program for Chongqing Overseas Returnees (No. CX2021018), Research Start-up Fund of Xi’an University of Architecture and Technology (No. 196032407) and Graduate Research and Innovation Foundation of Chongqing (No. CYB23026). We thank Miss Jiao’e Dang at Instrument Analysis Center of Xi’an University of Architecture and Technology for their assistance with SEM analysis. The authors also extend their gratitude to Shiyanjia Lab (www.shiyanjia.com) for their help with the FT-IR test.

Supplementary materials

Supplementary material associated with this article can be found, in the online version, at doi:10.1016/j.cclet.2025.111174.

References

[1] W. Wu, S. Wang, L. Lin, H.Y. Shi, X. Sun, Energy Environ. Sci. 16 (2023) 4326–4333.
[2] Q. Gou, H. Luo, L. Qu, et al., J. Energy Chem. 101 (2025) 191–200.
[3] S. Zhang, L. Chen, J. Xie, et al., Inorg. Chem. 61 (2022) 4561–4565.
[4] S. Zhang, Q. Gou, W. Chen, et al., Adv. Sci. 11 (2024) 2404968.
[5] Y. Su, B. Liu, Q. Zhang, et al., Adv. Funct. Mater. 32 (2022) 2204306.
[6] Y. Zou, Y. Wu, W. Wei, et al., Adv. Mater. 36 (2024) 2313775.
[7] Y. Su, B. Chen, Y. Sun, et al., Adv. Mater. 35 (2023) 2301410.
[8] W. Lyu, H. Fu, A.M. Rao, et al., Sci. Adv. 10 (2024) eadr9602.
[9] Q. Li, H. Wang, H. Yu, et al., Adv. Funct. Mater. 33 (2023) 2303466.
[10] M. Han, J. Yao, J. Huang, et al., Chin. Chem. Lett. 34 (2023) 107493.
[11] H. Luo, J. Deng, Q. Gou, et al., Chin. Chem. Lett. 34 (2023) 107885.
[12] C. Li, Z. Sun, T. Yang, et al., Adv. Mater. 32 (2020) 2003425.
[13] T. Shu, X. Yang, Z. Huang, et al., J. Mater. Chem. A 12 (2024) 4666–4677.
[14] Y. Zong, H. He, Y. Wang, et al., Adv. Energy Mater. 13 (2023) 2300403.
[15] Q. Gou, Z. Chen, H. Luo, et al., Small 20 (2024) 2305902.
[16] Q. Gou, H. Luo, Y. Zheng, et al., Small 18 (2022) 2201732.
[17] W. Wu, X. Yang, K. Wang, et al., Adv. Funct. Mater. 32 (2022) 2207397.
[18] Y. Chen, F. Gong, W. Deng, H. Zhang, X. Wang, Energy Stor. Mater. 58 (2023) 20–29.
[19] W. Deng, Z. Xu, G. Li, X. Wang, Small 19 (2023) 2207754.
[20] Y. Chen, K. Zhang, Z. Xu, et al., Energy Environ. Sci. 18 (2025) 713–727.
[21] J. Cao, M. Sun, D. Zhang, et al., ACS Nano 18 (2024) 16610–16621.
[22] Y. Han, F. Wang, L. Yan, et al., Chem. Sci. 15 (2024) 12336–12348.
[23] P. Sun, L. Ma, W. Zhou, et al., Angew. Chem. Int. Ed. 60 (2021) 18247–18255.
[24] X. Liu, Y. Fang, P. Liang, et al., Chin. Chem. Lett. 32 (2021) 2899–2903.
[25] K. Li, Z. Guo, Q. Sun, et al., Chem. Eng. J. 454 (2023) 140223.
[26] H. Luo, Q. Gou, Y. Zheng, et al., ACS Nano 19 (2025) 2427–2443.
[27] H. Yang, L. Li, D. Chen, et al., Angew. Chem. Int. Ed. 64 (2025) e202419394.
[28] N. Hu, W. Lv, W. Chen, et al., Adv. Funct. Mater. 34 (2024) 2311773.
[29] Z. Luo, Y. Xia, S. Chen, et al., Nano-Micro Lett. 15 (2023) 205.
[30] J. Li, Z. Guo, J. Wu, et al., Adv. Energy Mater. 13 (2023) 2301743.
[31] J. Wang, Y. Yu, R. Chen, et al., Adv. Sci. 11 (2024) 2402821.
[32] Y. Zhao, H. Hong, L. Zhong, et al., Adv. Energy Mater. 13 (2023) 2300627.
[33] K. Li, C. Yin, X. Dai, et al., J. Energy Storage 55 (2022) 105722.
[34] Y. Ai, C. Yang, Z. Yin, et al., J. Am. Chem. Soc. 146 (2024) 15496–15505.
[35] Q. Sun, Z. Guo, T. Shu, et al., ACS Appl. Mater. Interfaces 16 (2024) 12781–12792.
[36] S. Qi, J. Tian, J. Zhang, et al., CCS Chem. 4 (2022) 1850–1857.
[37] C. Li, Q. Gou, R. Tang, et al., J. Phys. Chem. Lett. 14 (2023) 9150–9158.
[38] X. Yang, W. Li, Z. Chen, et al., Angew. Chem. Int. Ed. 62 (2023) e202218454.
[39] H. Wang, W. Ye, B. Yin, et al., Angew. Chem. Int. Ed. 62 (2023) e202218872.
[40] A. Li, X. Zhang, Z. Xu, M. Wu, Chem. Eng. J. 494 (2024) 153240.
[41] G. Ma, L. Miao, Y. Dong, et al., Energy Stor. Mater. 47 (2022) 203–210.
[42] X. Wang, Y. Ying, X. Li, et al., Energy Environ. Sci. 16 (2023) 4572–4583.
[43] Y. Cao, X. Tang, L. Li, et al., Nano Res. 16 (2023) 3839–3846.
[44] K. Wang, T. Qiu, L. Lin, et al., ACS Energy Lett. 9 (2024) 1000–1007.
[45] D. Wang, Y. Xin, D. Yao, et al., Adv. Funct. Mater. 32 (2022) 2104162.

[46] J. Cao, D. Zhang, R. Chanajaree, et al., ACS Appl. Mater. Interfaces 15 (2023) 45045–45054.
[47] J. Luo, L. Xu, Y. Zhou, et al., Angew. Chem. Int. Ed. 62 (2023) e202302302.
[48] X. Gu, Y. Du, Z. Cao, et al., Chem. Eng. J. 460 (2023) 141902.
[49] X. Gong, H. Yang, J. Wang, G. Wang, J. Tian, ACS Appl. Mater. Interfaces 15 (2023) 4152–4165.
[50] J. Wan, R. Wang, Z. Liu, et al., ACS Nano. 17 (2023) 1610–1621.
[51] B. Liu, L. Yu, Q. Xiao, et al., Chem. Sci. 15 (2024) 16118–16124.
[52] K. Xie, K. Ren, Q. Wang, et al., eScience 3 (2023) 100153.
[53] K. Ren, M. Li, Q. Wang, et al., Nano-Micro Lett. 16 (2024) 117.
[54] W. Guo, L. Xu, Y. Su, et al., ACS Nano 18 (2024) 10642–10652.
[55] Z. Hou, T. Zhang, X. Liu, et al., Sci. Adv. 8 (2022) eabp8960.
[56] N. Guo, W. Huo, X. Dong, et al., Small Methods 6 (2022) 2200597.
[57] Y. Tao, Y. Cui, H. Wang, et al., Adv. Funct. Mater. 35 (2025) 2414805.
[58] R. Wang, J. He, C. Yan, et al., Adv. Mater. 36 (2024) 2402681.
[59] Y. Wang, K. Xue, X. Zhang, et al., Chem. Eng. J. 460 (2023) 141704.
[60] S. Zhang, J. Chen, W. Chen, et al., Angew. Chem. Int. Ed. 64 (2025) e202424184.